JGR Space Physics

RESEARCH ARTICLE
10.1029/2024JA032585

Waves and Instabilities in Saturn's Magnetosheath: 2. Dispersion Relation Analysis

I. Cheng[1], N. Achilleos[1], X. Blanco-Cano[2], C. Bertucci[3], and P. Guio[4]

[1]Department of Physics and Astronomy, University College London, London, UK, [2]Instituto de Geofísica, Universidad Nacional Autónoma de México, Mexico, DF, Mexico, [3]IAFE, UBA-CONICET, Buenos Aires, Argentina, [4]Department of Physics and Technology, Arctic University of Norway, Tromsø, Norway

Key Points:

- Dispersion solvers indicate ion cyclotron (IC) mode dominates over mirror mode (MM) at Saturn, but MM prevails with high O^+ abundance
- The predicted MM linear growth rates at Saturn were 0.02–0.2, exceeding the inferred maximum rate of 0.008 from observations
- The scale size of MM at maximum linear growth rate was 4–12 ρ_p, smaller than the inferred size of 18–38 ρ_p from observations

Correspondence to:
I. Cheng,
i.cheng.19@ucl.ac.uk

Citation:
Cheng, I., Achilleos, N., Blanco-Cano, X., Bertucci, C., & Guio, P. (2024). Waves and instabilities in Saturn's magnetosheath: 2. Dispersion relation analysis. *Journal of Geophysical Research: Space Physics*, *129*, e2024JA032585. https://doi.org/10.1029/2024JA032585

Received 18 MAR 2024
Accepted 6 SEP 2024

Author Contributions:
Supervision: N. Achilleos
Writing – original draft: I. Cheng

Abstract The WHAMP (Rönnmark, 1982, https://inis.iaea.org/search/search.aspx?orig_q=RN:14744092) and LEOPARD (Astfalk & Jenko, 2017, https://doi.org/10.1002/2016ja023522) dispersion relation solvers were used to evaluate the growth rate and scale size for mirror mode (MM) and ion cyclotron (IC) instabilities under plasma conditions resembling Saturn's magnetosheath in order to compare observations to predictions from linear kinetic theory. Instabilities and waves are prevalent in planetary magnetosheaths. Understanding the origin and conditions under which different instabilities grow and dominate can help shed light on the role each instability plays in influencing the plasma dynamics of the region. For anisotropic plasmas modeled with bi-Maxwellian particle distribution, the dispersion, growth rate, and scale size of MM and IC were studied as functions of proton temperature anisotropy, proton plasma beta, and oxygen ion abundance. The dispersion solvers showed that the IC mode dominated over MM under typical conditions in Saturn's magnetosheath, but that MM could dominate for high enough O^+ abundance (>40% n_e). These water ion-rich plasma conditions are occasionally found in Saturn's magnetosheath (Sergis et al., 2013, https://doi.org/10.1002/jgra.50164). The maximum linear growth rates (γ_m/Ω_p) for MM ranged from 0.02 to 0.2, larger than expected from observations. The scale size at maximum growth rate ranged from 4 to 12 ρ_p, smaller than expected from observations. These inconsistencies could potentially be attributed to diffusion and non-linear growth processes.

Plain Language Summary Plasma instabilities have well-defined relationships between the wavevector and the frequency captured in the dispersion relation. Linear kinetic theory provides a basis for interpreting instability growth rates and scale sizes in simulations and observations with small plasma fluctuations. However, it cannot describe the fate of the instability such as the maximum amplitude, nor its interactions with other modes. The ion cyclotron (IC) and mirror mode (MM) instabilities lead to fluctuations of different frequencies and spatial scales. Their growth occurs when the plasma exhibits temperature perpendicular-to-magnetic-field greater than some threshold of the temperature parallel-to-magnetic-field direction known as temperature anisotropy. Each instability has a role to play in influencing the plasma dynamics of the region. This study investigates the growth and scale size of IC and MM instabilities in conditions resembling Saturn's magnetosheath.

1. Introduction

Magnetosheaths are known to exhibit proton temperature anisotropy such that $T_\perp > T_\parallel$ (e.g., Tsurutani et al., 1982; Sergis et al., 2013), where $\perp$ and $\parallel$ indicate directions perpendicular and parallel, respectively, to the background field $\mathbf{B_0}$. This anisotropy could be produced during ion heating at the quasi-perpendicular bow shock (Thomsen et al., 1985), but is reduced as the plasma flows downstream (Sckopke et al., 1990) due to the presence of plasma instabilities or waves.

In an electron-proton plasma, $T_\perp > T_\parallel$ conditions may drive two electromagnetic modes below the proton gyrofrequency (Ω_p): the ion cyclotron (IC) and mirror instabilities, provided that the electron temperature is not much greater than the ion temperature (Gary, 1992) (i.e., a cold electron component). The mirror mode (MM) is a purely compressional mode with zero real frequency (i.e., non-oscillatory and non-propagating, but growing in time), and has a maximum growth rate (γ_m) oblique to the background magnetic field $\mathbf{B_0}$. The IC mode is a rotational mode with non-zero frequencies below the ion gyrofrequency (Ω_i) and has a maximum growth rate at propagation parallel to $\mathbf{B_0}$. The mode frequency plateaus as it approaches Ω_i due to being in resonance with ion gyration leading to damping of the wave and zero group velocity.

The temperature anisotropy threshold for the mirror instability is (Hasegawa, 1969):

$$\frac{T_\perp}{T_\parallel} > 1 + \frac{1}{\beta_\perp}, \quad (1)$$

where T is the ion temperature, β is the plasma beta, $\perp$ and $\parallel$ indicate perpendicular-to- and parallel-to-magnetic-field directions.

The strong pitch angle scattering produced by the IC instability (Machida et al., 1988) is expected to reduce the ion temperature anisotropy thus inhibiting the growth of MM which generally requires a higher anisotropy threshold than IC in an electron-proton plasma (Gary et al., 1976). However, Price et al. (1986) showed that the presence of small amounts of helium ions reduces the linear growth rate of IC significantly thus permitting the MM to dominate linear wave growth. Large amplitude MM waves can also produce field rotations that scatter ions non-adiabatically and reduce ion temperature anisotropy causing the instability to saturate quickly (McKean et al., 1993).

Some of the important parameters to compare between observations and theoretical models are the scale size (in terms of ion gyroradii ρ_i) and the linear growth rate (in terms of Ω_i) of the instabilities. This study uses linear dispersion relation solvers, WHAMP (Rönnmark, 1982) and LEOPARD (Astfalk & Jenko, 2017), to provide a basis for interpreting such parameters in future simulations and observations with small plasma and field fluctuations.

An intriguing question is, under what condition does MM dominate IC during the non-linear growth phase? However, this is beyond the scope of linear dispersion solvers which provide insight into the early stages of instability growth. The goal of the present study is to answer the following questions:

1. How do the maximum growth rates and scale size of MM and IC differ between WHAMP and LEOPARD dispersion solvers?
2. How does the growth rate of MM compete with IC under plasma conditions resembling Saturn's magnetosheath?
3. How do the maximum growth rates and scale sizes of MM obtained from WHAMP and LEOPARD compare to observations of MM waves in Saturn's magnetosheath?

2. Cassini Data Set

This study uses magnetic field and plasma data to extract distributions of Saturn's magnetosheath condition for input into the dispersion relation solvers. The data were obtained by three instruments on board Cassini: (a) The dual-technique magnetometer (MAG) (Dougherty et al., 2004). (b) The electron spectrometer (ELS) and the ion mass spectrometer (IMS) sensors of the Cassini Plasma Spectrometer (CAPS) instrument (Young et al., 2004). (c) The charge-energy-mass spectrometer (CHEMS) and the low energy magnetospheric measurements system (LEMMS) sensors of the Cassini magnetospheric imaging instrument (MIMI) (Krimigis et al., 2004). All data were obtained from the Planetary Plasma Interactions (PPI) Node of the Planetary Data System (PDS).

The data set of MM events was the same as that used in a companion study (Cheng et al., 2024) on MM waves in Saturn's magnetosheath. The events were extracted from 1,589 magnetosheath intervals made by the Cassini spacecraft between 27 June 2004 and 29 May 2012, when plasma data from the CAPS instrument were broadly available.

3. Methods

The frequencies and growth rates of the competing MM and IC instabilities were calculated using two different dispersion relation solvers: Waves in Homogeneous Anisotropic Magnetized Plasma (or WHAMP) (Rönnmark, 1982) which treats ions with mass but electrons as massless particles, and Linear Electromagnetic Oscillations in Plasmas with Arbitrary Rotationally-symmetric Distributions (or LEOPARD) (Astfalk & Jenko, 2017) which treats both ions and electrons as particles with mass.

For MM, it was required that the mode frequency $\omega_r \approx 0$ for all k for a large angle of propagation relative to the background magnetic field. The propagation angle at maximum growth rate decreased with increasing anisotropy,

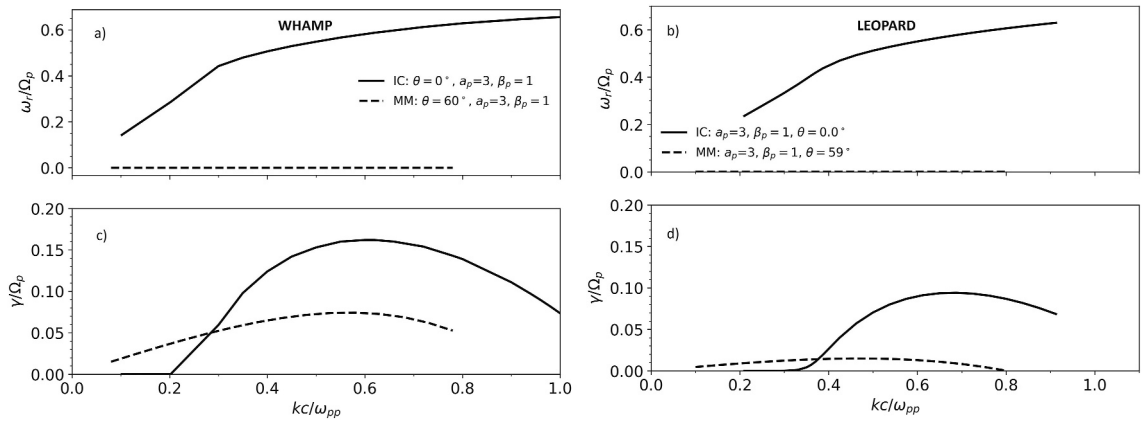

Figure 1. The frequency (a, b) and growth rate (c, d) of the mirror mode (MM) and ion cyclotron instabilities as a function of wavenumber at proton temperature anisotropy of $a_p = 3$. The proton plasma $\beta_p = 1$, $T_e/T_{\|p} = 1$, $B = 2$ nT, $n_p = 0.1\,\mathrm{cm}^{-3}$ and $v_A/c = \Omega_p/\omega_{pp} = 4.6 \times 10^{-4}$ is the ratio of gyro frequency to plasma frequency which gives a measure for the magnetisation and density of the plasma. The two propagation angles for the MM in WHAMP and LEOPARD correspond to the MM maximum growth rate.

varying from $\theta_{Bk} = 71°$ to $\theta_{Bk} = 63°$ for anistropy values between 2 and 2.5 (Gary, 1992). For the IC mode, it was required that $\omega_r < \Omega_p$ at parallel propagation $\theta_{Bk} = 0°$ (Gary, 1992). The resulting dispersion relation (ω vs. k) was validated against the Alfvén/IC (A/IC) branch such as in Figure 1 of Krauss-Varban et al. (1994).

The maximum growth rate (γ_m), and the corresponding frequency (ω_m) and wavenumber (thus scale size $\lambda_m = 2\pi/k_m$) were evaluated as a function of temperature anisotropy (a_p), plasma β and fraction of heavy ion components (n_O/n_e) to compare with observations. These calculations were done under plasma conditions resembling Saturn's magnetosheath as obtained from Cassini data. For plots of dispersion relation results, all frequencies were normalized to the proton gyrofrequency Ω_p and lengths were scaled to the proton gyroradius ρ_p. Note that in WHAMP lengths were also scaled to the proton gyroradius $\rho_p = v_p/\Omega_p$ where v_p is the proton thermal velocity (Rönnmark, 1982). In LEOPARD, all lengths were scaled to the ion inertial length $d_i = c/\omega_{pp}$ where ω_{pp} is the proton plasma frequency (Astfalk & Jenko, 2017).

The anisotropy values investigated were between 1 and 100, motivated by the anisotropy distribution estimated from the magnetosheath magnetic field and electron number density data using the relation given in Hasegawa (1969).

$$\frac{\delta n}{n} = \left(1 - \frac{T_\perp}{T_\|}\right)\frac{\delta B}{B}, \tag{2}$$

where $T_\perp/T_\|$ is the ratio of perpendicular to parallel temperature relative to the direction of the background magnetic field.

The plasma β values investigated were between 1 and 10, motivated by its distribution in the magnetosheath.

At Saturn, there is a frequent presence of high-energy water-group ions (called W^+) within the magnetosheath plasma which have been leaked from the magnetosphere and escape both downstream within the magnetosheath and upstream into the unshocked solar wind (Sergis et al., 2013). To model this heavy-ion leakage, oxygen ion (O^+) of mass 16 was introduced to the mixture as a third component to investigate its effect on IC and MM growth rates. For context, a 5% O^+ and 95% H^+ ions mixture in a plasma with the electron number density of $10^5\ \mathrm{m}^{-3}$ would give O^+ number density of $5 \times 10^3\ \mathrm{m}^{-3}$, whilst a more extreme 50% O^+ would give $5 \times 10^4\ \mathrm{m}^{-3}$, both of which are within the observed number densities in Saturn's magnetosheath (Cheng et al., 2024). Thus, the range 5%–50% O^+ was used for this investigation.

The input parameters used in the dispersion solvers are summarized in Table 1.

Table 1
Input Parameters for Dispersion Solvers. "-" Entries Mean Species Not Used

Case	Comment	Species	β_i	B (nT)	m_1 (m_p)	n_1 (cm^{-3})	T_1 (eV)	a_1	v_{d1}	m_2 (m_p)	n_2 (cm^{-3})	T_2 (eV)	a_2	v_{d2}	m_3 (m_p)	n_3 (cm^{-3})	T_2 (eV)	a_3	v_{d3}
1	Vary a	1_p, 2_e	1	2	1	0.1	100	2, 10	0	0	0.1	$T_{p,\|}$	1	0	–	–	–	–	–
2	Vary T	1_p, 2_e	1, 100	2	1	0.1	100, 10,000	3	0	0	0.1	$T_{p,\|}$	1	0	–	–	–	–	–
3	Vary n and T	1_p, 2_O, 3_e	3	2	1	0.095, 0.05	315, 600	3	0	16	0.005, 0.05	6,000, 600	3	0	0	0.1	$T_{p,\|}$	1	0

Note. Entries with comma-separated values indicate the range of values over which to vary the parameter. These parameters are indicated in the "Comment" column. The β_i column represents the plasma β of all the ion species in the mixture.

In all the experiments with WHAMP and LEOPARD, the electron temperature T_e was set to the parallel proton temperature $T_{p,\|}$, following the treatment in Gary (1992). However, the equivalent experiments were performed with $T_e = 0.1\mathrm{T_p}$ as informed by magnetosheath data, but these had quantitatively similar results as $T_e = T_{p,\|}$.

For comprehensive details on these dispersion solvers, we refer the reader to documentation on WHAMP (Rönnmark, 1982) and LEOPARD (Astfalk & Jenko, 2017).

4. Results and Discussion

First, the results from both WHAMP and LEOPARD are reported and compared. Then, the ability of MM to compete against IC under a range of plasma conditions resembling Saturn's magnetosheath is assessed. Finally, observations of MM wave growth rates and scale sizes in Saturn's magnetosheath are put into context by comparing them with those obtained from WHAMP and LEOPARD.

4.1. Dispersion Analysis: WHAMP and LEOPARD

All frequencies and growth rates are relative to the proton gyrofrequency (Ω_p) and wavenumbers are relative to the ratio of proton plasma frequency to the speed of light ω_{pp}/c, unless otherwise stated. In general, both WHAMP and LEOPARD showed much of the same trend in how the frequency and growth rate varied with wavenumber for MM and IC, and that the MM growth dominated over IC at smaller wavenumbers. However, under the same conditions, LEOPARD produced growth rates that were lower than WHAMP for both MM and IC. Growth rates for MM solutions generally decreased to zero or negative values as the propagation angle increased toward 90°, which agrees with Huddleston et al. (1999). Note that both dispersion solvers start at the same point from the general dispersion equation and the aim is to find non-trivial solutions of $\vec{E}(\omega, k)$. However, the method of solving such an equation differs in the two dispersion solvers. WHAMP introduces the Padé approximation to solve the general dispersion equation. This method uses a sum of rational polynomials of a given order to estimate a function near a specific point instead of requiring function derivatives as in the Taylor series. On the other hand, LEOPARD uses a polynomial fit, specifically Muller's method, to solve the general dispersion equation. These different numerical techniques can yield varying results due to rounding and truncation errors in computation.

Examples of dispersion relation and growth rate against wavenumber for WHAMP and LEOPARD are plotted in Figure 1). The input plasma consisted of proton and electron components whose parameters are described in detail in the figure caption. The expected real frequencies of each mode were obtained: less than the proton gyrofrequency Ω_p for IC and zero for MM. The growth rates are smaller in LEOPARD than in WHAMP, and the maximum linear growth rate occurs at slightly different wavenumbers for both solvers.

4.1.1. Linear Maximum Growth Rate

In a proton-electron plasma, the MM maximum growth rate was lower than that of IC for all values of anisotropy tested, and both modes' maximum growth rate increased with anisotropy as seen in Figures 2c and 2d. In

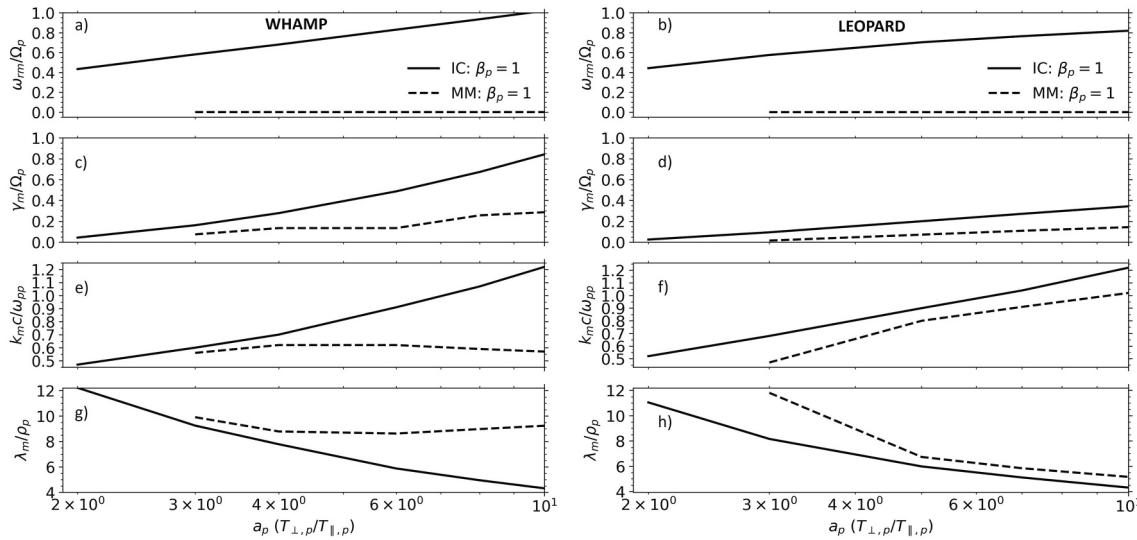

Figure 2. Plot of maximum growth rate γ_m with corresponding frequency, wavenumber and wavelength against anisotropy. The proton $\beta_p = 1$. For ion cyclotron, the propagation angle was 0° for both solvers. For mirror mode, the propagation angles were 60° and 59° in WHAMP and LEOPARD, respectively.

WHAMP, the MM maximum growth rate varied from 0.05 to 0.2, and in LEOPARD, from 0.02 to 0.15, for a_p = 3–10.

Southwood and Kivelson (1993), Equation 7 and 12 provide analytical expressions for the MM growth rate under the fluid and kinetic treatments in the $k_\parallel^2 \ll k_\perp^2$ limit, respectively. However, given that the propagation angles used in this study were not very close to 90°, these analytical expressions were not used to make a comparison of the growth rates.

Electrons were kept isotropic in all the experiments. Although electron anisotropy could be gained at the bow shock, they are expected to scatter to isotropy much quicker compared to ions. Although not possible to verify using Cassini data due to limited pitch angle coverage, other observational studies such as Gosling et al. (1989) showed that the core thermal electron distribution was roughly isotropic inside Earth's magnetosheath.

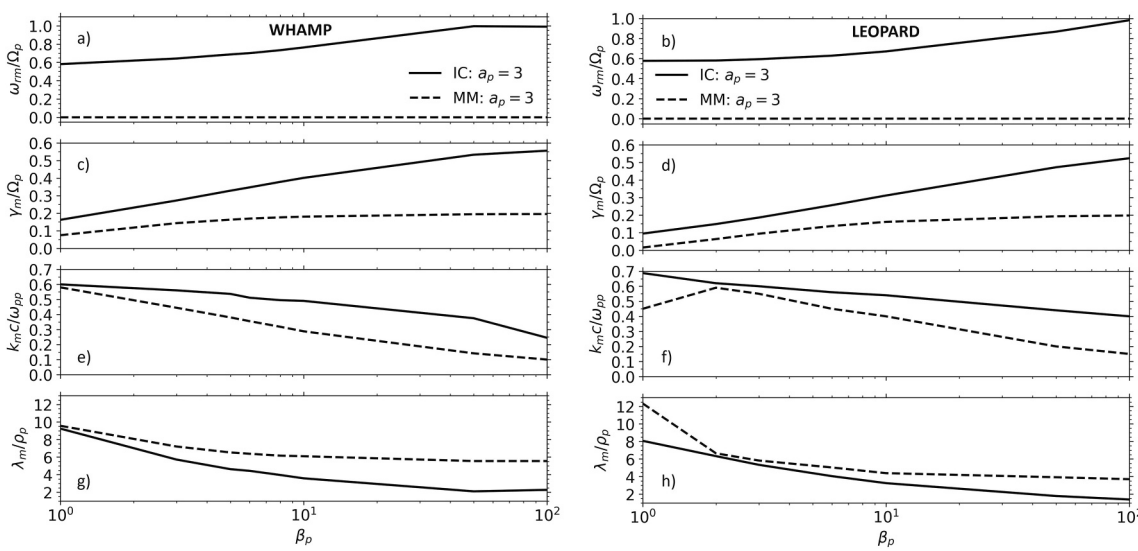

Figure 3. Plot of maximum growth rate γ_m with corresponding frequency, wavenumber and wavelength against β_p. The proton temperature anisotropy was $T_\perp/T_\parallel = 3$. For ion cyclotron, the propagation angle was 0° for both solvers. For mirror mode, the propagation angles were 60° and 59° in WHAMP and LEOPARD, respectively.

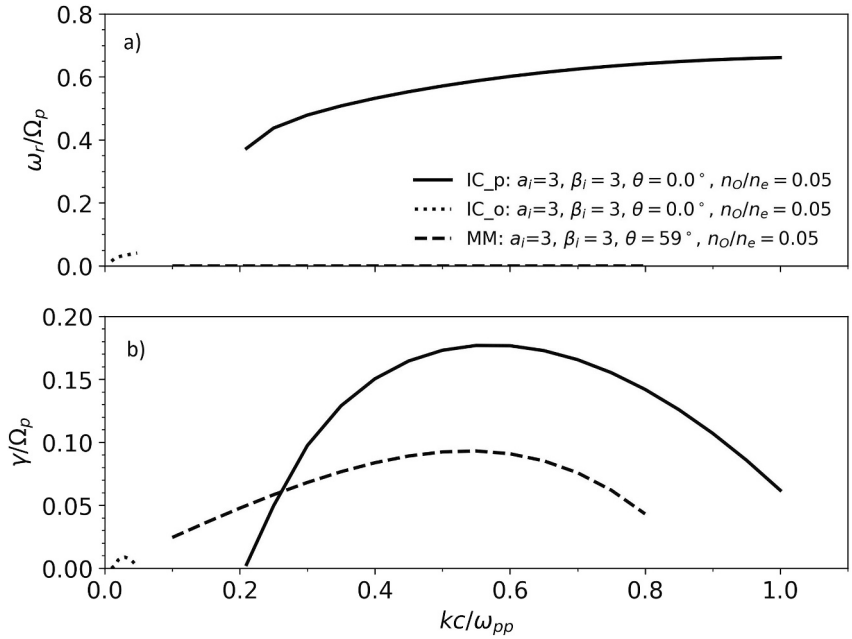

Figure 4. The frequency (a) and growth rate (b) of the mirror mode (MM) and ion cyclotron (IC) mode for proton and oxygen as a function of wavenumber. The proton and oxygen anisotropies were both $T_\perp/T_\parallel = 3$, proton β_p and oxygen β_O were both 3, the propagation angle of IC and MM were 0° and 59° respectively, and O^+ ion abundance was $0.05n_e$. This plot was produced using results from LEOPARD.

Figure 3c and d show how the maximum growth rate varies with proton plasma β_p from 1 to 100 with anisotropy $a_p = 3$. In LEOPARD, the maximum growth rate of MM was found to increase from 0.02 to 0.20. The MM growth rate remained lower than IC for the domain tested. The same trend was observed in WHAMP but at higher growth rates for lower values of β. The effect of increasing plasma β lowers the anisotropy threshold for the plasma to become mirror unstable (Equation 1), which is expected to allow the mode to grow faster under the same anisotropy (Gary et al., 1976, Figure 3).

The effect of oxygen ion (O^+) abundance on the maximum growth rate γ_m was investigated by varying n_O/n_e from 5% to 50% whilst reducing the proton abundance from 95% to 50% to maintain the neutrality of the plasma. For this plasma mixture, the solution for an oxygen IC wave was also found (Figure 4) at a frequency ∼16 times lower than the proton IC due to $m_O = 16m_p$. Figure 5c and d show that the maximum growth rate of the proton IC mode decreased rapidly from 0.18 to 0.05 as the abundance of O^+ increased from 5% to 50%. In contrast, the MM growth rate was relatively insensitive to the increase of O^+ decreasing only marginally from 0.09 to 0.08. At 40% oxygen, the maximum growth rates for IC and MM become the same at ∼0.85. As the oxygen abundance increases at the expense of the protons, the rapid decrease in the maximum growth rate of the proton IC mode is due to fewer protons resonating with the proton IC mode. However, the maximum growth rate of the oxygen IC mode remained substantially lower than that of proton IC and MM for the range of n_O/n_e tested. At $n_O/n_e = 0.5$, when both the proton and O^+ temperatures are the same $(\beta_p = \beta_{O^+} = 3)$, the scale size of the MM ∼ 8–10 ρ_p becomes comparable to the O^+ gyroradius ∼4 ρ_p. Their similarity in scale size could impact the energy transfer of oxygen gyromotion to the oxygen IC mode. These must remain speculative statements until further analysis takes place.

In a simulation study of MM growth at Earth by McKean et al. (1993), the authors investigated two classes of linear growth times: slow and fast. The minimum linear growth time (Equation 3) can be compared with the proton cyclotron period $T_c = 2\pi/\Omega_p$ to indicate slow or fast growth. If $\tau \approx T_c$ the wave is undergoing fast growth regime. Otherwise, $\tau > T_c$ is the slow growth regime. The authors found that an initial proton anisotropy of $T_\perp/T_\parallel \approx 2$ produced MM in the slow growth regime with $\tau \sim 5\ T_c$, and took a time of $t \sim 16T_c = 48$ s to reach linear saturation (i.e., largest amplitude in the linear growth phase). When the anisotropy was increased to $T_\perp/T_\parallel \approx 6$, the MM was in the fast growth regime with $\tau \sim 1\ T_c$, taking a time of $t \sim 5\ T_c = 15$ s to reach the end of the linear

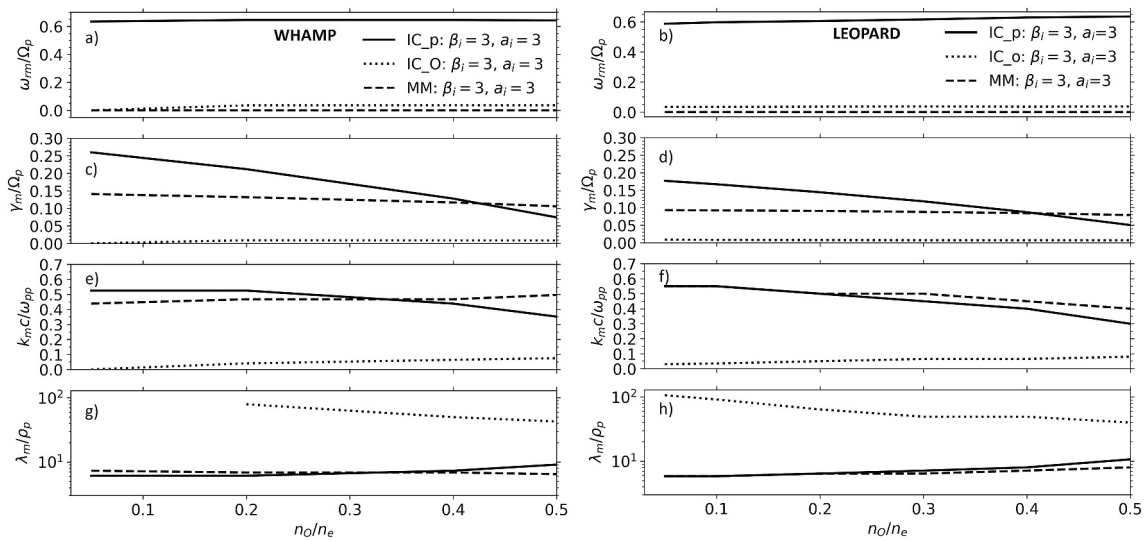

Figure 5. Plot of maximum growth rate γ_m and the corresponding wavenumber against the abundance of O^+ ions from 0.05 n_e to 0.5 n_e. The proton and oxygen anisotropies were both $T_\perp/T_\parallel = 3$, proton β_p and oxygen β_O were both 3, and the propagation angle of ion cyclotron and mirror mode were 0° and 59° for LEOPARD and 0° and 60° for WHAMP respectively.

growth phase. In both cases, the value of proton cyclotron period T_c in Earth's magnetosheath was ~3 s, based on a field strength of 20 nT.

For this study, the ratio τ/T_c is given by Ω_p/γ, where Ω_p is in Hz. This is known from the maximum growth curves obtained from the dispersion solver. For a proton-electron plasma mixture under conditions typical in Saturn's magnetosheath (see Table 1), and the linear growth time was $\tau > T_c$ for the anisotropy values tested, putting the MM growth rate at Saturn in the slow growth regime. Our estimate of the linear growth time is $\tau \approx T_c = 30$ s and is expected to last a couple of T_c (McKean et al., 1993). The estimated time to reach non-linear saturation is up to 3,000 s indicating that linear growth saturation could be reached soon downstream of BS as suggested by Cattaneo et al. (1998), but non-linear growth may continue for a much longer period of time within the magnetosheath.

Since peaks represent the non-linear saturation phase of MM growth (Joy et al., 2006), Cheng et al. (2024) found that peak non-linear saturation is reached at a distance ~5 R_S from the BS where the MM peaks occurrence reaches a maximum. This could indicate a region in Saturn's magnetosheath with maximum temperature anisotropy which could be confirmed with anisotropy data on a future Saturn mission. For a magnetosheath flow speed of $v_{SH} = 100\,\mathrm{km\,s^{-1}}$ and B = 2 nT, giving $T_c = 30$ s, this distance corresponds to a total growth time of $t = 5R_S/v_{SH} \approx 100T_c \approx 3000$ s, which is 100× larger than the linear growth time $\tau = 30$.

4.1.2. Scale Size at Maximum Growth Rate

Figures 2e–2h show the wavenumber and scale size λ_m corresponding to the maximum growth rate γ_m for anisotropy $a_p = 1$–100 at $\beta_p = 1$. There is a difference in the trend for scale size at maximum growth between the two dispersion solvers. WHAMP predicts the scale sizes of the MM structures to remain at around $10\rho_p$, whilst LEOPARD predicts their scale size to decrease from 12 ρ_p to around 5 ρ_p, between anisotropy values of 3–10. However, in both solvers, the MM scale size is larger than that of IC for all values of anisotropy tested.

The effect of proton plasma β_p on the scale size λ_m at maximum growth was investigated and shown in Figures 3e–3h. Keeping B = 2 nT, β_p was increased from 1 to 100 by increasing the temperature of protons T_p, whilst keeping the number density constant. The scale size of both MM and IC in terms of gyroradius ρ_p decreased because ρ_p increased with T_p. The range of scale sizes for MM was 4–12 ρ_p, and for IC it was 3–9 ρ_p. The scale size of IC was consistently smaller than MM for all values of β_p tested.

Figures 5e–5h show the effect of O^+ abundance on the scale size of IC and MM at maximum growth. In LEOPARD, the presence of O^+ tends to increase the scale size for both the proton IC and MM modes, and

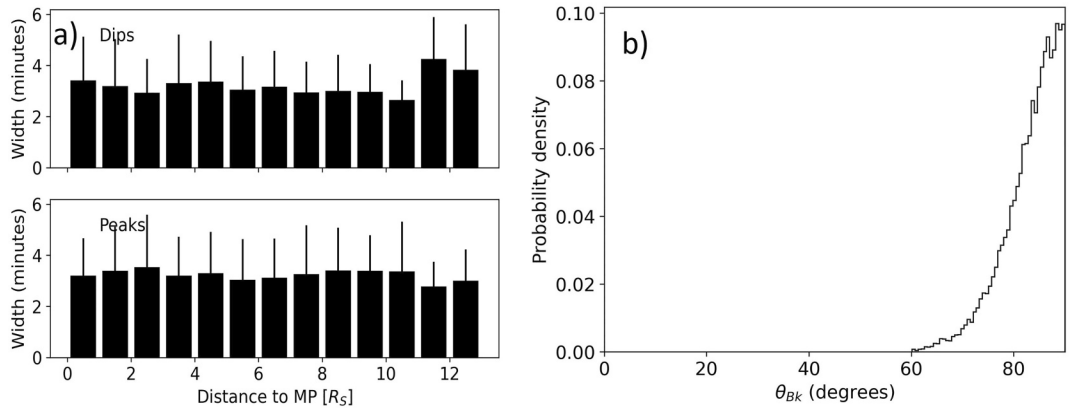

Figure 6. Characteristics of mirror mode (MM) waves in Saturn's magnetosheath where Cassini traversed from bow shock to magnetopause or vice versa. (a) Bar plot (with uncertainty) of the duration of MM peaks and dips as a function of distance from the magnetopause, in 1 R_S bins. (b) Distribution of θ_{Bk} angle between the background magnetic field vector and the minimum variance direction.

decrease the scale size for the oxygen IC mode. Both MM and IC have the same scale sizes of 6–7 ρ_p between 5% and 20% O^+. Beyond 20% O^+, the scale size of IC increased faster and reached 11 ρ_p whilst MM reached 8 ρ_p, at 50% O^+. For the oxygen IC mode, the scale size decreased from 110 ρ_p to 40 ρ_p. In WHAMP, the proton IC scale size had similar values. In contrast, the MM scale size decreased from 7.5 to 6.5 ρ_p as oxygen abundance increased from 5% to 50%.

4.2. Observations of Mirror Mode Waves

4.2.1. Scale Size of MM Waves

One of the important parameters to compare between observations and theoretical models is the scale size of stable MM structures such as magnetic "dips" (Joy et al., 2006) in terms of ion gyroradii, defined as the distance across the MM structure (perpendicular to the background field).

The median width in the duration of all MM waves in Saturn's magnetosheath was 3 min. For dips and peaks, the mean duration across all magnetosheath traversals were 3.2 ± 1.5 minutes and 3.2 ± 1.65 minutes respectively. These values were similar for MM waves found in different types of magnetosheath traversals. This timescale is in good agreement with the results of Russell et al. (2008, Figure 1), where they showed an increasing width in time of MM waves seen by Helios, Pioneer Venus, Ulysses and Cassini from 0.34 to 8.9 AU.

Figure 6a shows that the width of dips and peaks including uncertainty was rather uniform across all distances to MP. The mean duration of MM dips and peaks remained at 3 min across all distances to the MP, within an uncertainty of around a minute. This was somewhat unexpected as Hasegawa and Tsurutani (2011) described a diffusion process that causes the wave to expand from the source to the observation point. The two larger bars at the end of the "dips" panel consisted of 14 events, all of which were located in the dawn (6.2–8.2 local hours) and dusk (15–16.1 local hours) sectors. The magnetosheath size in these regions may be larger and more variable due to the flaring of the BS and MP. The field lines and MM structures may be oriented in a more tail-ward direction along the flanks, thus Cassini likely observed longer-duration MM structures as they are being advected downstream. Furthermore, MM waves found in the magnetosheath flanks were more likely to be "dips" (Joy et al., 2006; Soucek et al., 2008, 2015). The flanks correspond to regions downstream of quasi-parallel shock where the temperature is less anisotropic. Thus, these "dips" may correspond to MM that originated from quasi-perpendicular magnetosheath regions. In Joy et al. (2006), MM dips were attributed to the collapse phase of the MM. During this phase, the perturbed magnetic field returns to the background state, and only some inflated magnetic bottles remain, which are observed as dips.

Assuming non-drifting MM waves and negligible spacecraft velocity (~few km s^{-1}), the plasma velocity vector perpendicular to the background field should be used when converting time to distance across the MM structure as θ_{Bk} was close to perpendicular. However, given that plasma velocity data was only good about half the time, we

Table 2
The Observed Scale Sizes of Mirror Mode Structures in Various Planetary Magnetosheaths

Magnetosheath environment	MM scale size (ρ_p)	Sources
Earth	20	Tsurutani et al. (1982)
	10	Horbury and Lucek (2009)
Mars	>16	Jin et al. (2022)
	10–20	Wedlund et al. (2022)
Jupiter	25	Tsurutani et al. (1982)
	20	Erdős and Balogh (1996)
Saturn	40	Tsurutani et al. (1982); Violante et al. (1995)
	18–38	Cheng et al. (2024)
Comet Halley	8	Russell et al. (1991)

Note. Most studies did not state where in the magnetosheaths the measurements were made, what field strength was used for the proton gyroradius, nor what the uncertainties were.

used the limited data available to determine the average angle between the 10-min averaged magnetic field and plasma flow. The mean angle θ_{Bk} was 80° for over 4,500 individual MM dips and peaks (Figure 6b), imposing little correction to the flow speed. However, the spread was rather large with a standard deviation of 44°. For comparison, this angle at Jupiter was about 70°, with no uncertainty quoted (Erdős & Balogh, 1996).

The typical field strength of 2 nT and a probable proton temperature of 200 eV with a corresponding thermal speed of $\sim$200km s^{-1} (assuming $a_p = 1$) would give a proton gyroradii $\rho_p = 1000$ km. However, if the typical MM dip minimum field strength of 1 nT was used, the gyroradius doubles to $\rho_p = 2000$ km. Since we expect the magnetosheath to have temperature anisotropy greater than one, the gyroradius would become even larger. However, note that a larger temperature anisotropy does not necessarily increase ρ_p in the WHAMP linear dispersion analysis results as the gyroradius in WHAMP is defined with respect to the proton thermal velocity with proton temperature $T_p = m_p v_p^2/2$ (Rönnmark, 1982).

Using typical magnetosheath flow speeds of 178, 226 and 272 km s^{-1} found in (Cheng et al., 2024), and a duration of 3.2 min, the corresponding scale sizes of MM waves in terms of the smaller proton gyroradius for $B = 2$ nT would be 28, 32 and 38 ρ_p, respectively. If the larger gyroradii were used for $B = 1$ nT, the scale sizes would be 18, 20 and 24 ρ_p, respectively.

These scale sizes were in good agreement with $\sim 29\rho_p$ predicted by Hasegawa and Tsurutani (2011), at a magnetosheath distance 1/3 along the Sun-Saturn line from the bow shock to the magnetopause due to Bohm-like diffusion; a process similar to an expanding "smoke ring." Using values in this study to evaluate Eq. 9 in their paper, $\Omega_p = 0.09$ s^{-1} for 1 nT field, magnetosheath thickness is $\sim 10R_S = 6.0 \times 10^5$ km, a magnetosheath flow speed of 227 km s^{-1}, a new prediction for the scale size becomes $\sim 17\rho_p$. Here, one of the sources of uncertainty is the magnetosheath thickness as it is estimated from models of the bow shock and magnetopause boundaries.

For comparison with previous observational studies, MM scale size in Saturn's magnetosheath was 40 ρ_p based on a larger field strength of 4 nT (Tsurutani et al., 1982; Violante et al., 1995). In Jupiter's magnetosheath, the average width of the MM structures was 20 ρ_p (Erdős & Balogh, 1996). For Mars' magnetosheath, MAVEN data revealed a scale size between 10 and 20 proton gyroradii behind a quasi-perpendicular bow shock (Jin et al., 2022; Wedlund et al., 2022). For Earth's magnetosheath, it was between 10 and 20 ρ_p based on a field strength of 20 nT and proton temperature of 170 eV (Horbury & Lucek, 2009; Tsurutani et al., 1982). At comet Halley, MMs have an average scale size of a water-group ion gyro diameter (Russell et al., 1991), or 8 ρ_p, assuming protons and oxygen have the same temperature and anisotropy. A summary of these scale sizes and their sources is given in Table 2.

We now compare results from the linear dispersion relation solvers (Section 4.1.2) and observations. For the range of conditions examined, the scale sizes at maximum growth for MM, ranged from $\sim 4\,\rho_p$ to 12 ρ_p, with an average

of 8 ρ_p. Observations showed that the scale sizes of MM ranged from ~18–38 ρ_p which is several times larger than the predictions obtained from the dispersion solvers.

A possible explanation is the Bohm-like diffusion mechanism described in Hasegawa and Tsurutani (2011) that shifts the spectra to lower wavenumbers as the mode is advected away from the source to the observation point. Erdős and Balogh (1996) suggested that the proton gyroradius ρ_p should be calculated with the suprathermal population such that on average it might be a factor of 3 larger. Applying this correction to the observed MM scale sizes shifts the values closer to that expected from linear kinetic theory. Other reasons may include an overestimation of the magnetosheath speed, lack of correction for spacecraft speed and trajectory across the MM structure was not taken into account; and a correct determination of the width requires accurate knowledge of the plasma and spacecraft velocities. These aspects and other possible causes would be interesting avenues for future quantitative and hybrid simulation investigations of MM scale sizes.

4.2.2. Growth Rate of MM Waves

Erdős and Balogh (1996) suggested that since the minimum variance direction of MM structures is almost perpendicular to the background magnetic field, the size of the weak field region would be much larger in the direction along the field line than across it. The authors argued that to maintain pressure balance, the particles need sufficient time to travel to the weak field region as the MM grows. This sets a lower limit on the linear growth time

$$\tau_{\min} = 1/\gamma_m, \tag{3}$$

to be the time taken for protons to traverse along the length $L = w \tan\theta_{Bk}$ of the MM from strong to weak field region, where w is the width of the MM, and θ_{Bk} is the angle between the background magnetic field vector and the minimum variance direction. In terms of an upper limit on the growth rate,

$$\gamma_m = \frac{v_{th,p}}{w \tan\theta_{Bk}}, \tag{4}$$

where $v_{th,p}$ is the proton thermal speed. Using $\rho_p = 2000$ km for B = 1 nT, width $w = 24\rho_p \approx 48000$ km and an average $\theta_{Bk} = 80°$ (Figure 6b), the MM length L is about 272,000 km. Assuming 200 eV protons with a thermal speed of 200 km s^{-1}, those with zero pitch angle will travel fastest into the weak field region and would take ~1360 s to complete the journey along the whole MM bottle (≈20 gyro periods for gyrofrequency $\Omega_p = 0.096$ rad s^{-1}). In other words, the MM growth rate (γ_m) should be less than $\gamma_m/\Omega_p \approx 0.008$.

Overall, the maximum linear growth rates ranging from 0.02 to 0.2 obtained from the dispersion solvers under conditions expected in Saturn's magnetosheath is much larger than the maximum growth rate of 0.008 expected from data following pressure balance arguments (Erdős & Balogh, 1996). However, as explained in Section 4.2.1, the upper limit of growth rate is so small due to the large longitudinal distance of the MM which has likely undergone Bohm-like diffusion as explained by Hasegawa and Tsurutani (2011) and is in the non-linear growth stage. Therefore, the disagreement between the linear growth rates and expected growth rates from observations should not be much of a surprise.

5. Conclusions

An analysis of MM and IC dispersion was performed using two dispersion relation solvers: WHAMP and LEOPARD, highlighting their differences. The competition between the growth of MM and IC in Saturn's magnetosheath was assessed. Finally, observations of MM waves' scale size and growth rates were put into context by comparing them with results from the linear dispersion analysis. The main findings were:

1. **Dispersion solver**: LEOPARD generally produced lower growth rates than WHAMP for both IC and MM under the same conditions. The IC mode dominates over MM under typical Saturn magnetosheath conditions, but MM can dominate for high enough O^+ abundance. These water ion-rich plasma conditions are occasionally found in Saturn's magnetosheath (Sergis et al., 2013). The maximum linear growth rates (γ_m/Ω_p) for MM ranged from 0.02 to 0.2, larger than expected from observations. The scale size at maximum growth rate

ranged from 4 to 12 ρ_p, smaller than expected from observations. These inconsistencies could potentially be attributed to diffusion and non-linear growth processes.

2. **Observations**: MM scale size ranged from 18 to 38 ρ_p depending on the field strength used for the proton gyroradius ρ_p. The maximum growth rate γ_m/Ω_p was estimated to be 0.008. The time taken to reach non-linear saturation was $t \approx 100T_c \approx 3{,}000$ s.

The difference between observations and predictions could be due to inhomogeneities such as density gradients and non-Maxwellian velocity distribution functions of the real Saturn magnetosheath whilst linear dispersion solvers assume homogeneous Maxwellian distributions. This work also led to new questions: Which mode dominates in Saturn's magnetosheath, IC or MM? Are the IC wave scale size and growth rate in line with that predicted by linear dispersion solvers? Answering these questions would require the identification of IC waves using magnetic spectrograms which provide information about the frequency of fluctuations. In addition, why does the MM scale size not vary with distance from the MP if diffusion-like processes are expected to cause them to expand? To further understand the causes of these observations, non-linear analytical and numerical models should be used to consider the effects of heavy ions and suprathermal particles (of Kronian origin) on the growth rates of MM and IC. 3D hybrid simulations of MM and IC could shed new light on the non-linear growth and saturation processes (e.g., Shoji et al., 2012). Ultimately, the combination of numerical studies and simulations would further our understanding of the nature and evolution of anisotropic instabilities like MM and IC in planetary magnetosheaths and other space plasma environments.

Data Availability Statement

The list of bow shock and magnetopause boundary crossings is available at https://github.com/ikitcheng/BS_MP_Crossings_Cassini, where a detailed list of changes made may also be found. These were characterised by using the Cassini MAG and ELS data available from the PDS (https://pds.nasa.gov/).

Acknowledgments
IKC was supported by a UK STFC studentship hosted by the UCL Centre for Doctoral Training in Data Intensive Science (grant number ST/P006736/1). NA was supported by UK STFC Consolidated Grant number ST/S000240/1 (UCL/MSSL-Physics and Astronomy Solar System). XBC was supported by PAPIIT DGAPA grant IN110921. The authors wish to thank William Dunn for his invaluable discussions and constructive comments about this work.

References

Astfalk, P., & Jenko, F. (2017). LEOPARD: A grid-based dispersion relation solver for arbitrary gyrotropic distributions. *Journal of Geophysical Research: Space Physics*, *122*(1), 89–101. https://doi.org/10.1002/2016ja023522

Cattaneo, M. B. B., Basile, C., Moreno, G., & Richardson, J. D. (1998). Evolution of mirror structures in the magnetosheath of Saturn from the bow shock to the magnetopause. *Journal of Geophysical Research: Space Physics*, *103*(A6), 11961–11972. https://doi.org/10.1029/97ja03683

Cheng, I., Achilleos, N., Blanco-Cano, X., Bertucci, C., Sergis, N., Paranicas, C., & Guio, P. (2024). Waves and instabilities in Saturn's magnetosheath: 1 Mirror mode waves and their impact on magnetopause reconnection. *Journal of Geophysical Research: Space Physics*.

Dougherty, M. K., Kellock, S., Southwood, D. J., Balogh, A., Smith, E. J., Tsurutani, B. T., et al. (2004). The Cassini magnetic field investigation. *Space Science Reviews*, *114*(1–4), 331–383. https://doi.org/10.1007/s11214-004-1432-2

Erdős, G., & Balogh, A. (1996). Statistical properties of mirror mode structures observed by Ulysses in the magnetosheath of Jupiter. *Journal of Geophysical Research: Space Physics*, *101*(A1), 1–12. https://doi.org/10.1029/95ja02207

Gary, S. P. (1992). The mirror and ion cyclotron anisotropy instabilities. *Journal of Geophysical Research*, *97*(A6), 8519–8529. https://doi.org/10.1029/92ja00299

Gary, S. P., Montgomery, M. D., Feldman, W. C., & Forslund, D. W. (1976). Proton temperature anisotropy instabilities in the solar wind. *Journal of Geophysical Research*, *81*(7), 1241–1246. https://doi.org/10.1029/ja081i007p01241

Gosling, J. T., Thomsen, M. F., Bame, S. J., & Russell, C. T. (1989). Suprathermal electrons at earth's bow shock. *Journal of Geophysical Research: Space Physics*, *94*(A8), 10011–10025. https://doi.org/10.1029/ja094ia08p10011

Hasegawa, A. (1969). Drift mirror instability in the magnetosphere. *Physics of Fluids*, *12*(12), 2642–2650. https://doi.org/10.1063/1.1692407

Hasegawa, A., & Tsurutani, B. T. (2011). Mirror mode expansion in planetary magnetosheaths: Bohm-like diffusion. *Physical Review Letters*, *107*(24), 245005. https://doi.org/10.1103/physrevlett.107.245005

Horbury, T. S., & Lucek, E. A. (2009). Size, shape, and orientation of magnetosheath mirror mode structures. *Journal of Geophysical Research: Space Physics*, *114*(A5). https://doi.org/10.1029/2009ja014068

Huddleston, D. E., Strangeway, R. J., Blanco-Cano, X., Russell, C. T., Kivelson, M. G., & Khurana, K. K. (1999). Mirror-mode structures at the galileo-io flyby: Instability criterion and dispersion analysis. *Journal of Geophysical Research: Space Physics*, *104*(A8), 17479–17489. https://doi.org/10.1029/1999ja900195

Jin, T., Lei, L., Yiteng, Z., Lianghai, X., & Fuhao, Q. (2022). Statistical analysis of the distribution and evolution of mirror structures in the Martian magnetosheath. *The Astrophysical Journal*, *929*(2), 165. https://doi.org/10.3847/1538-4357/ac5f00

Joy, S. P., Kivelson, M. G., Walker, R. J., Khurana, K. K., Russell, C. T., & Paterson, W. R. (2006). Mirror mode structures in the Jovian magnetosheath. *Journal of Geophysical Research*, *111*(A12). https://doi.org/10.1029/2006ja011985

Krauss-Varban, D., Omidi, N., & Quest, K. B. (1994). Mode properties of low-frequency waves: Kinetic theory versus hall-mhd. *Journal of Geophysical Research: Space Physics*, *99*(A4), 5987–6009. https://doi.org/10.1029/93JA03202

Krimigis, S. M., Mitchell, D. G., Hamilton, D. C., Livi, S., Dandouras, J., Jaskulek, S., et al. (2004). Magnetosphere imaging instrument (MIMI) on the Cassini mission to Saturn/titan. *Space Science Reviews*, *114*(1–4), 233–329. https://doi.org/10.1007/s11214-004-1410-8

Machida, S., Goertz, C. K., & Hada, T. (1988). The electromagnetic ion cyclotron instability in the Io torus. *Journal of Geophysical Research: Space Physics*, *93*(A7), 7545–7550. https://doi.org/10.1029/ja093ia07p07545

McKean, M. E., Gary, S. P., & Winske, D. (1993). Kinetic physics of the mirror instability. *Journal of Geophysical Research*, *98*(A12), 21313–21321. https://doi.org/10.1029/93ja01993

Price, C. P., Swift, D. W., & Lee, L.-C. (1986). Numerical simulation of nonoscillatory mirror waves at the earth's magnetosheath. *Journal of Geophysical Research*, *91*(A1), 101–112. https://doi.org/10.1029/ja091ia01p00101

Rönnmark, K. (1982). *Whamp-waves in homogeneous, anisotropic, multicomponent plasmas (Tech. Rep.)*. Kiruna Geofysiska Inst. https://inis.iaea.org/search/search.aspx?orig_q=RN:14744092

Russell, C. T., Jian, L. K., Luhmann, J. G., Zhang, T. L., Neubauer, F. M., Skoug, R. M., et al. (2008). Mirror mode waves: Messengers from the coronal heating region. *Geophysical Research Letters*, *35*(15). https://doi.org/10.1029/2008gl034096

Russell, C. T., Le, G., Schwingenschuh, K., Riedler, W., & Yeroshenko, Y. (1991). Mirror mode waves at comet Halley. In *Cometary plasma processes* (pp. 161–169). American Geophysical Union. https://doi.org/10.1029/gm061p0161

Sckopke, N., Paschmann, G., Brinca, A. L., Carlson, C. W., & Lühr, H. (1990). Ion thermalization in quasi-perpendicular shocks involving reflected ions. *Journal of Geophysical Research: Space Physics*, *95*(A5), 6337–6352. https://doi.org/10.1029/ja095ia05p06337

Sergis, N., Jackman, C. M., Masters, A., Krimigis, S. M., Thomsen, M. F., Hamilton, D. C., et al. (2013). Particle and magnetic field properties of the Saturnian magnetosheath: Presence and upstream escape of hot magnetospheric plasma. *Journal of Geophysical Research: Space Physics*, *118*(4), 1620–1634. https://doi.org/10.1002/jgra.50164

Shoji, M., Omura, Y., & Lee, L. (2012). Multidimensional nonlinear mirror-mode structures in the earth's magnetosheath. *Journal of Geophysical Research: Space Physics*, *117*(A8). https://doi.org/10.1029/2011ja017420

Soucek, J., Escoubet, C. P., & Grison, B. (2015). Magnetosheath plasma stability and ULF wave occurrence as a function of location in the magnetosheath and upstream bow shock parameters. *Journal of Geophysical Research: Space Physics*, *120*(4), 2838–2850. https://doi.org/10.1002/2015ja021087

Soucek, J., Lucek, E., & Dandouras, I. (2008). Properties of magnetosheath mirror modes observed by cluster and their response to changes in plasma parameters. *Journal of Geophysical Research: Space Physics*, *113*(A4). https://doi.org/10.1029/2007ja012649

Southwood, D. J., & Kivelson, M. G. (1993). Mirror instability: 1. Physical mechanism of linear instability. *Journal of Geophysical Research*, *98*(A6), 9181–9187. https://doi.org/10.1029/92ja02837

Thomsen, M. F., Gosling, J. T., Bame, S. J., & Mellott, M. M. (1985). Ion and electron heating at collisionless shocks near the critical Mach number. *Journal of Geophysical Research: Space Physics*, *90*(A1), 137–148. https://doi.org/10.1029/ja090ia01p00137

Tsurutani, B. T., Smith, E. J., Anderson, R. R., Ogilvie, K. W., Scudder, J. D., Baker, D. N., & Bame, S. J. (1982). Lion roars and nonoscillatory drift mirror waves in the magnetosheath. *Journal of Geophysical Research*, *87*(A8), 6060–6072. https://doi.org/10.1029/ja087ia08p06060

Violante, L., Cattaneo, M. B. B., Moreno, G., & Richardson, J. D. (1995). Observations of mirror waves and plasma depletion layer upstream of Saturn's magnetopause. *Journal of Geophysical Research*, *100*(A7), 12047–12055. https://doi.org/10.1029/94ja02703

Wedlund, C. S., Volwerk, M., Mazelle, C., Halekas, J., Rojas-Castillo, D., Espley, J., & Möstl, C. (2022). Making waves: Mirror mode structures around mars observed by the MAVEN spacecraft. *Journal of Geophysical Research: Space Physics*, *127*(1). https://doi.org/10.1029/2021ja029811

Young, D. T., Berthelier, J. J., Blanc, M., Burch, J. L., Coates, A. J., Goldstein, R., et al. (2004). Cassini plasma spectrometer investigation. *Space Science Reviews*, *114*(1–4), 1–112. https://doi.org/10.1007/s11214-004-1406-4